Original Article

Integrated analysis reveals prognostic correlation and immune characteristics of a tumor-associated macrophage-based risk signature in triple-negative breast cancer

Shichen Miao[1#], Chengyu Bian[2#], Jun Fang[1#], Shanshan Wang[3#], Huan You[1], Yi Zhou[1], Qichao Ni[1]

[1]Department of Thyroid and Breast Surgery, Affiliated Hospital of Nantong University, Medical School of Nantong University, Nantong, China; [2]Department of Thoracic Surgery, The First People's Hospital of Changzhou and The Third Affiliated Hospital of Soochow University, Changzhou, China; [3]Department of General Surgery, The Affiliated Suqian Hospital of Xuzhou Medical University and Nanjing Drum Tower Hospital Group Suqian Hospital, Suqian, China

Contributions: (I) Conception and design: S Miao, C Bian, Q Ni; (II) Administrative support: Q Ni; (III) Provision of study materials or patients: J Fang, Q Ni; (IV) Collection and assembly of data: S Miao, S Wang; (V) Data analysis and interpretation: S Miao, C Bian; (VI) Manuscript writing: All authors; (VII) Final approval of manuscript: All authors.

[#]These authors contributed equally to this work as co-first authors.

Correspondence to: Qichao Ni, PhD. Department of Thyroid and Breast Surgery, Affiliated Hospital of Nantong University, Medical School of Nantong University, 20 Xisi Road, Nantong 226001, China. Email: nqcuser@163.com.

Background: Tumor-associated macrophages play a critical role in the progression and immune response of triple-negative breast cancer (TNBC). Our study aimed to explore the characteristics of tumor-associated macrophages (TAMs) in TNBC, construct a risk signature associated with TAM clusters, and verify its relationship with prognosis and immune-related characteristics.

Methods: Firstly, we identified four TAM clusters and determined prognosis-related clusters in TNBC based on the single-cell RNA sequencing (scRNA-seq) data. Subsequently, the TAM-related prognostic genes were obtained by the univariate Cox regression analysis and an 8-gene risk signature was then constructed by least absolute shrinkage and selection operator (LASSO) regression based on these TAM-related prognostic genes. Analyses of immune characteristics showed a significant association between the signature with stromal and immune scores, as well as some immune cells.

Results: Multivariate analysis revealed that the risk signature was an independent prognostic factor for TNBC, and its value in predicting immunotherapeutic outcomes was also confirmed. A novel nomogram integrating the stage and TAM-based risk signature was constructed, which exhibited favorable predictability and reliability in the prognosis prediction of TNBC. Finally, the increasing expression of *GPR34* which is one of the eight hub genes was explored in TNBC by experiments including reverse-transcriptase polymerase chain reaction, western blot, and immunohistochemistry.

Conclusions: Our study may provide unique insights into obtaining independent prognostic factors, improving immunotherapeutic strategies, and identifying effective therapeutic targets for TNBC.

Keywords: Tumor-associated macrophage (TAM); triple-negative breast cancer (TNBC); *GPR34*; risk signature

Submitted Jun 22, 2024. Accepted for publication Sep 14, 2024. Published online Oct 29, 2024.
doi: 10.21037/tcr-24-1037
View this article at: https://dx.doi.org/10.21037/tcr-24-1037

Introduction

Breast cancer is the most prevalent malignancy and the leading cause of cancer-related death among women worldwide. In 2020, it was estimated that there were 2.3 million new cases and over 685,000 deaths attributed to breast cancer (1). Among the different subtypes, triple-negative breast cancer (TNBC) represents approximately 20% of cases and is known for its aggressive nature, high recurrence rates, and mortality (2,3). The absence of the estrogen receptor (ER) and progesterone receptor (PR) and lack of human epidermal growth factor receptor 2 (HER2) amplification preclude TNBC patients from benefiting from molecularly targeted therapies such as endocrine therapy and anti-HER2 therapy (1,3). In addition, only 5–10% of TNBC patients showed a response to standard chemotherapy (4). Thus, advances in therapeutic options and the search for more effective therapeutic targets for TNBC are urgently needed.

Recent progression in cancer immunotherapy has revolutionized cancer treatment paradigms (5). Characterized by higher immunogenicity compared with other breast cancer subtypes suggests immunotherapy is a viable strategy for TNBC (6). In contrast to other cancer types, the effectiveness of immunotherapy in breast cancer, including TNBC, has been relatively limited (7). Although immune checkpoint inhibitors (ICIs) have been utilized as a treatment option, the prognosis for advanced TNBC remains poor, especially for a small subset of TNBC patients with programmed cell death ligand-1 (PD-L1) expression, with a median overall survival (OS) of less than 2 years (6,7). Therefore, it is necessary to find new immunotherapy strategies for TNBC.

Tumor-associated macrophagesare crucial drivers of the immunosuppressive microenvironment and mediate tumor progression and resistance to immunotherapies (8,9). Modifying the properties and function of TAMs in malignancies can enhance tumor immune surveillance and suppress immunological evasion (8). TAMs have been proven to boost TNBC progression (10). It is illustrated that TAMs promote tumor-derived colony stimulating factor 1 (CSF-1) and macrophage-derived epidermal growth factor (EGF) release in TNBC (9). However, the specific features of TAMs and their relationship with the prognosis and immune-related characteristics of TNBC have not been thoroughly studied.

For decades, the emergence of single-cell technologies has attributed to dissecting the constellation of cell states of immune cells in the tumor microenvironment (TME) (5). Our exploration primally identified 4 TAM clusters based on scRNA-seq data and selected TAM clusters associated with TNBC prognosis subsequently. Then, we established an 8-gene risk signature based on the differentially expressed genes (DEGs) associated with these prognosis-related TAM clusters; the prognostic value and immune characteristics of the risk signature were further analyzed, and potentially effective breast cancer immunotherapy drugs were found based on this signature. Our study may provide new insight for updating the prognosis assessment methods and immunotherapy approaches for breast cancer. We present this article in accordance with the MDAR and TRIPOD reporting checklists (available at https://tcr.amegroups.com/article/view/10.21037/tcr-24-1037/rc).

Highlight box

Key findings

- We constructed an 8-gene tumor-associated macrophage (TAM)-based risk signature that effectively predicts the prognosis and immunotherapeutic outcomes in triple-negative breast cancer (TNBC) patients.

What is known and what is new?

- TAMs are known to influence the progression and immune evasion in cancers, including TNBC.
- This manuscript introduces a novel 8-gene risk signature based on TAM clusters.

What is the implication, and what should change now?

- The potential prognostic value of *GPR34* deserves further study.

Methods

Data acquisition and processing

We obtained scRNA-seq data (GSE206638) from the GEO database (https://www.ncbi.nlm.nih.gov/geo/), comprising 4 tumor and 3 juxta tumor (JT) samples of TNBC (11). Single cells were selected based on gene expression in a minimum of 3 cells and each cell expressing at least 250 genes. The bulk RNA-seq datasets which include survival data were collected from TCGA-BRCA and GSE58812 databases. Additionally, The PD-(L)1 treated dataset as well as its clinical traits were downloaded from the IMvigor210 cohort (12). The study was conducted in accordance with the Declaration of Helsinki (as revised in 2013).

Definition of TAM

To conduct a comprehensive analysis of TNBC scRNA-seq data and delve into the TAM signature, we utilized the "Seurat" package (13). Data preprocessing steps involved the exclusion of cells with gene expression counts below 250 or exceeding 6,000. Subsequently, log-normalization was performed on the remaining expressed genes. The FindIntegrationAnchors function was employed, and data dimensionality was reduced using UMAP algorithm. TAMs were identified based on four marker genes (*CD68*, *C1QA*, *APOC1*, and *CD163*), and subsequently re-clustered using FindClusters and FindNeighbors functions. We defined marker genes for each TAM cluster by employing the "FindAllMarkers" function, which compared different clusters using specific criteria including minpct =0.35, log fold change (FC) =0.5, and adjust P value <0.05. To analyze the copy number variation (CNV) characteristics of TAM clusters and differentiate them from tumor cells and normal cells, we utilized the "CopyKAT" package. Lastly, we performed Kyoto Encyclopedia of Genes and Genomes (KEGG) enrichment analysis on the marker genes using the "clusterProfiler" package (14).

Identification of hub genes of TAM

Initially, we utilized the "limma" package to identify DEGs between tumor and normal tissue (15). DEGs were selected based on a false discovery rate (FDR) of <0.05 and $|\log_2 FC| > 1$. Subsequently, we examined the correlations between DEGs and TAM clusters, identifying key TAM-related genes with P<0.001 and cor >0.4. Prognosis-related genes were determined using univariate Cox regression analysis from the "survival" package, considering P<0.05. To reduce the number of genes, LASSO Cox regression analysis was performed, followed by multivariate Cox regression analysis using a stepwise regression method. Finally, the predictive performance of the risk signature was evaluated using the receiver operating characteristic (ROC) curve analysis with the assistance of the "timeROC" package.

Immune landscape analysis

In the TCGA cohort, we evaluated the proportions of 22 immune cell subtypes using the CIBERSORT algorithm, which provides insights into immune cell infiltration (16). Furthermore, we utilized the ESTIMATE algorithm to calculate immune and stromal scores, enabling a deeper exploration of the TME. To validate differences in immune status between subtypes, we performed ESTIMATION analysis and single-sample gene set enrichment analysis (ssGSEA) (17,18). These analyses allowed us to gain a better understanding of the immune characteristics and microenvironmental differences among the subtypes.

Construction of a risk signature and nomogram

To develop a nomogram model for clinical application, we conducted univariate and multivariate Cox regression analyses on clinicopathological factors and risk signatures. The significant variables from the multivariate Cox model (P<0.05) were used to construct the nomogram using the "rms" package (19). Calibration curves were employed to assess the predictive accuracy of the model, and decision curve analysis (DCA) was utilized to evaluate its reliability. CCLs' drug sensitivity data were obtained from the Cancer Therapeutics Response Portal (CTRP v.2.0, released October 2015, https://portals.broadinstitute.org/ctrp) and PRISM Repurposing dataset (19Q4, released December 2019, https://depmap.org/portal/prism/). CTRP covers 481 compounds across 835 CCLs, PRISM includes 1,448 compounds across 482 CCLs. Both datasets use area under the dose-response curve (AUC) values to indicate drug sensitivity, with lower AUC values suggesting higher sensitivity. K-nearest neighbor (k-NN) imputation addressed missing AUC values, excluding compounds with over 20% missing data. Molecular data from CCLE, the source of CCLs in both datasets, were used for subsequent analyses.

RNA extraction and RT-PCR

Total RNA in cells (MDA-MB-231 and MCF-10A) was extracted according to the RNA-Quick Purification Kit (EScience, RN001, Shanghai, China). Complementary DNAs (cDNAs) were then synthesized by the HiScript III RT SuperMix for qPCR using 1 mg of total RNAs. Reverse-transcriptase polymerase chain reaction (RT-PCR) was performed using ChamQ Universal SYBR qPCR Master Mix (Vazyme, Q711, Shanghai, China) on a LightCycler96 (Roche, Shanghai, China) according to the kit instructions. Primer sets targeting mRNAs are listed in Table S1. We chose the housekeeping gene ACTB as an internal control.

Western blot

Protein was first extracted from MDA-MB-231 and MCF-10A with RIPA buffer (NCM Biotech, WB3100, Shanghai, China) containing protease inhibitors (Epizyme Biomedical Technology, GRF101, Shanghai, China). Protein samples were separated on 10% gels (Epizyme Biomedical Technology), then transferred to polyvinyl difluoride membranes. After being blocked in 5% nonfat dry milk, the membranes were then incubated at 4 ℃ in primary antibody against GPR34 (Abnova, PAB26304, Shanghai, China) overnight followed by incubation in HRP-conjugated secondary antibody (Beyotime, A0208, Shanghai, China) for 1 hour at room temperature. The bands were visualized through ECL (NCM Biotech, P10300, Shanghai, China) and imaged on a Bio-Rad image system. The signal intensity was quantified by ImageJ software (National Institutes of Health).

Immunohistochemistry

The tissue microarray sections (15 TNBC tumor tissues, 15 non-cancerous breast tissues) were deparaffinized and rehydrated: two changes of xylene for 5 min each; 100% alcohol, 95% alcohol, and 70% alcohol, each for 1 min, and then rinsed in distilled water, followed by Antigen retrieval (#S1699, Agilent Dako, Shanghai, China). After blocking the tissues, the primary antibody, *GPR34* (Abnova, PAB26304), was applied at 1:200 dilution, overnight at 4 ℃. The secondary antibody was incubated at room temperature for 30 min. The antibody binding was visualized using diaminobenzidine (DAB), resulting in the detection of the target protein. The breast cancer tissue and paracancer tissue were taken from the department of Thyroid and Breast Surgery, Affiliated Hospital of Nantong University, Medical School of Nantong University.

Immunofuorescence (IF)

Following fixation, permeabilization, and blocking, the tissues were incubated with primary antibodies, followed by incubation with secondary antibodies. The tissues were then stained with DAPI, and images were captured using a fluorescence microscope.

Statistical analysis

Statistical analyses were performed using R software (v4.1.2). Pearson or Spearman correlation was employed for correlation matrices, while the Wilcoxon test compared groups. Survival differences were assessed using Kaplan-Meier curves and the log-rank test, considering a P value <0.05 as statistically significant.

Results

Screening the TAMs in scRNA-seq samples

The flow chart of this study was shown in Figure S1. This study utilized scRNA-seq data and initially obtained 11,535 cells following screening. After log-normalization and dimensionality reduction, we identified 24 subpopulations. Subsequently, TAM populations were distinguished using four marker genes (*CD68*, *C1QA*, *APOC1*, and *CD163*) in Figure S2A,S2B. Further clustering and dimensionality reduction of TAM populations resulted in the identification of four TAM clusters, as shown in Figure S2C,S2D. The UMAP plot in *Figure 1A* demonstrated the distribution of seven samples, and ultimately, four TAM clusters were generated for subsequent analysis (*Figure 1B*). The initial violin plot displayed the manifestation of four markers within 24 clusters, while the second plot exhibited the expression of the same four markers in four distinct TAM subtypes. It was evident that the classification of TAMs was based on macrophages (Figure S3A,S3B). *Figure 1C* displayed the expression of the top five DEGs, acting as marker genes for TAM clusters. The proportion of the four clusters in each sample was illustrated in *Figure 1D*. KEGG analysis (*Figure 1E*) revealed enrichment of DEGs in various pathways, such as oxidative phosphorylation, Parkinson's disease, and prion disease. Additionally, based on CNV characteristics, the four TAM clusters encompassed 1,533 tumor and normal cells (*Figure 1F*).

The expression of cancer-related pathways in TAM

To investigate the association between TAM clusters and tumor progression, we examined ten tumor-related pathways within these clusters. *Figure 2A* showcased the gene set variation analysis (GSVA) scores of these pathways across different TAM clusters. Notably, the TAM-1 cluster exhibited a significantly higher ratio of malignant cells compared to the other clusters (*Figure 2B*). Moreover, GSVA scores of the tumor-related pathways differed between malignant and non-malignant cells within each TAM cluster (*Figure 2C*). Prognosis-associated ssGSEA

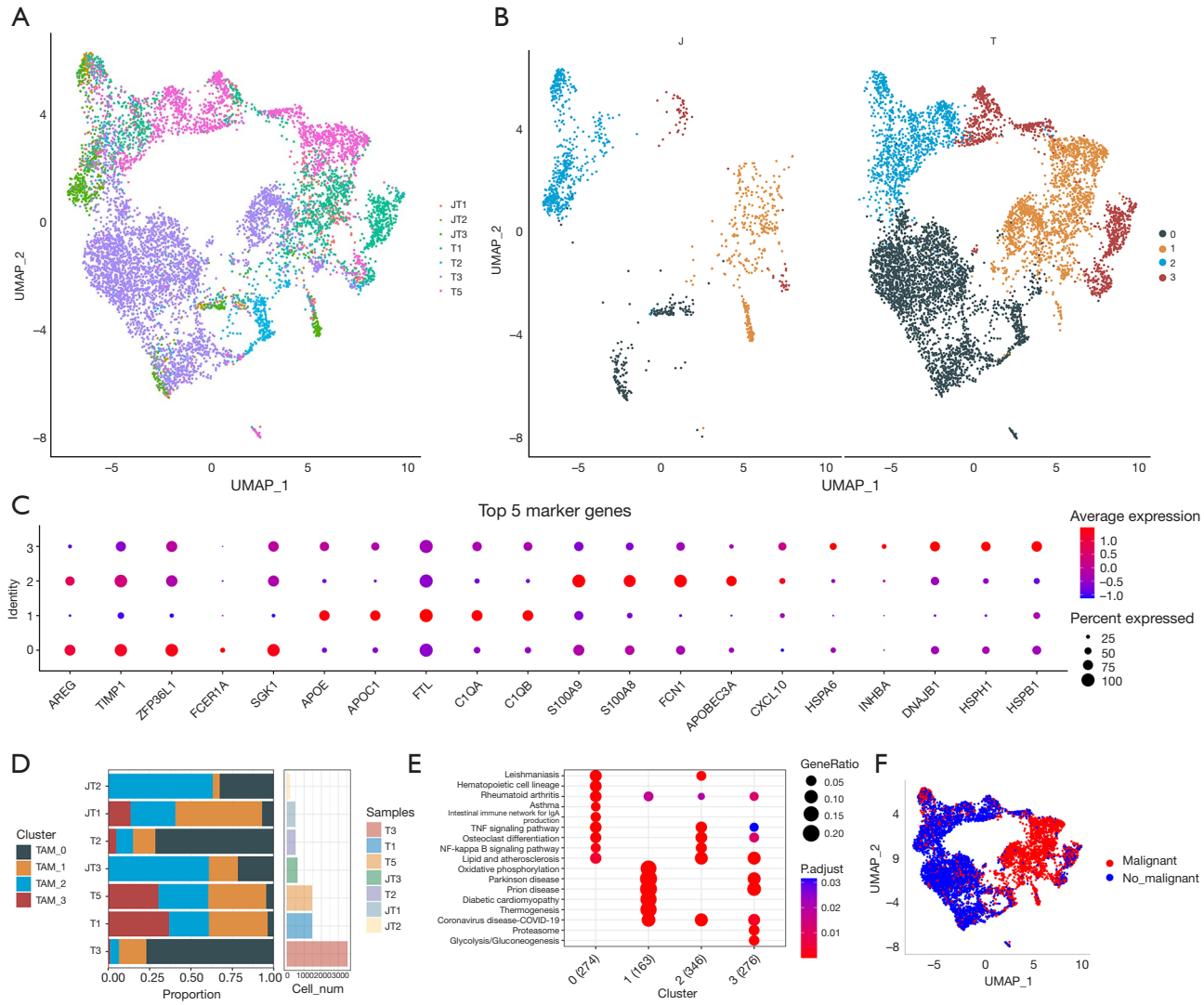

Figure 1 The identification of TAM clusters based on scRNA-seq data of TNBC patients. (A) UMAP plot of the distribution of 7 samples; (B) UMAP plot of the distribution of four clusters; (C) dot plot of the top 5 marker gene expressions of subgroups; (D) proportion and cell number of 4 subgroups in cancer and adjacent tissue; (E) KEGG enrichment analysis of 4 TAM subsets; (F) UMAP of malignant and non-malignant cells predicted by "copycat" package. TNBC, triple-negative breast cancer; TAM, tumor-associated macrophage; UMAP, uniform manifold approximation and projection; KEGG, Kyoto Encyclopedia of Genes and Genomes; scRNA-seq, single-cell RNA sequencing.

scores were calculated for marker genes of each TAM cluster using the TCGA cohort. Results indicated that TAM-1 and TAM-3 clusters had higher scores in tumor samples, while the opposite trend was observed in the remaining clusters (*Figure 2D*). By dividing TNBC samples into high- and low-TAM score groups, we found that the high-TAM score group exhibited a better prognosis in the TAM-1 and TAM-3 cluster, suggesting its potential significance in TNBC progression (*Figure 2E*).

Identification of hub genes associated with TAM

For the construction of a risk signature, DEGs between tumor and normal tissues were initially identified based on TCGA database. As shown in *Figure 3A*, a total of 2,160 DEGs were obtained, with 893 up-regulated DEGs and 1,267 down-regulated DEGs. Among them, 434 genes exhibited significant correlations with prognosis-related TAM clusters. Subsequently, univariate Cox

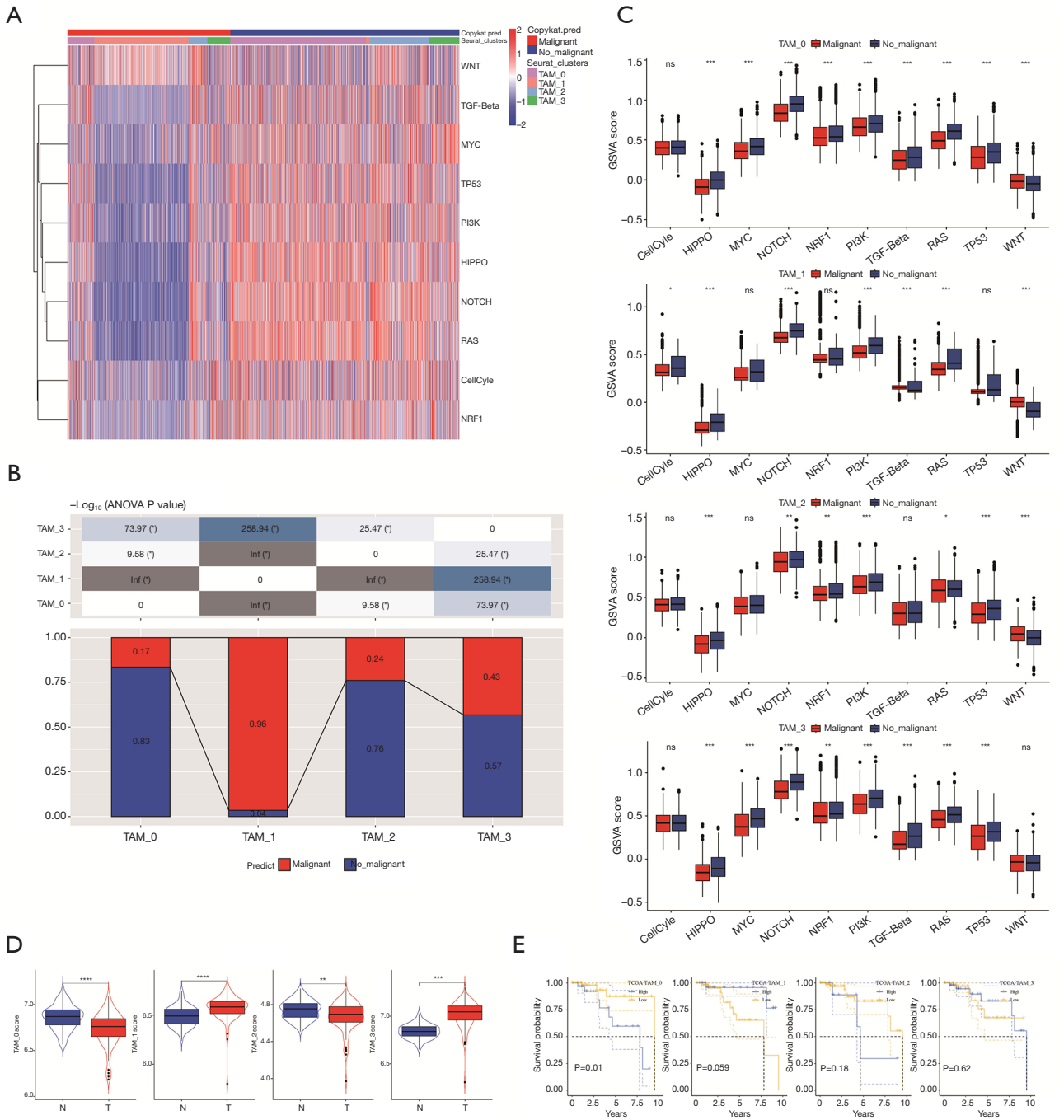

Figure 2 The tumor-related pathways and prognosis associated with four TAM clusters. (A) Heatmap of 10 tumor-related pathway scores enriched in TAMs; (B) comparison of TAM clusters in malignant and non-malignant cells; (C) comparison of GSVA score of each pathway between malignant and non-malignant cells in each cluster; (D) comparison of four TAM scores in cancer (T) and normal (N) tissues; (E) Kaplan-Meier curves of the high and low TAM score groups in each cluster. *, P<0.05; **, P<0.01; ***, P<0.001; ****, P<0.0001; ns, not significant. TAM, tumor-associated macrophage; GSVA, gene set variation analysis.

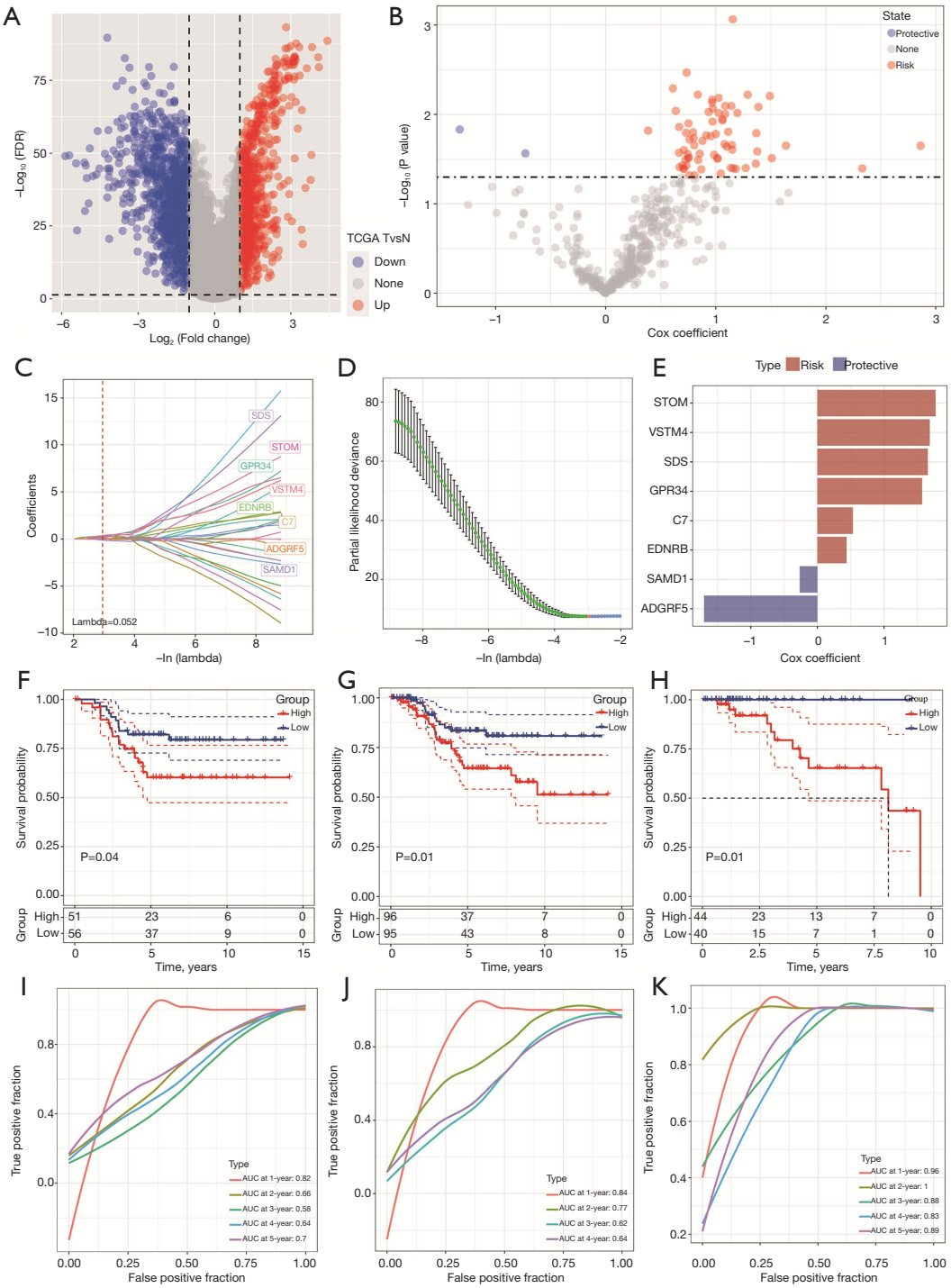

Figure 3 Identification of the hub predictive genes to construct a risk signature. (A) Volcano plot of differentially expressed genes of cancer and normal tissues in TCGA cohort; (B) volcano plot of prognosis-related genes identified from univariate Cox regression analysis; (C) the trajectory of each independent variable with lambda; (D) plots of the produced coefficient distributions for the logarithmic (lambda) series for parameter selection (lambda); (E) the multivariate Cox coefficients for each gene in the risk signature. Kaplan-Meier curves of risk model constructed by 8 genes in TCGA cohort (F), GEO cohort (G), and the meta cohort (H). ROC curves of risk model constructed by 8 genes in TCGA cohort (I), GEO cohort (J), and meta cohort (K). FDR, false discovery rate; GEO, Gene Expression Omnibus; TCGA, The Cancer Genome Atlas; ROC, receiver operating characteristic; AUC, area under the curve.

regression analysis assessed the prognostic value of each gene, resulting in 234 genes with prognostic significance (*Figure 3A*,*3B*). LASSO Cox regression analysis further narrowed down the gene selection to eight candidates (lambda =0.052) (*Figure 3C*,*3D*). Finally, a multivariate Cox regression analysis with stepwise regression yielded the inclusion of *ADGRF5*, *C7*, *EDNRB*, *GPR34*, *SAMD1*, *SDS*, *STOM*, and *VSTM4* in the risk signature (*Figure 3E*). The formula for the 8-gene signature was determined, and risk scores were calculated for each sample, subsequently dividing them into high- and low-risk groups after z-mean normalization. The final 8-gene signature formula is as follows: RiskScore =–1.700909607 × *ADGRF5* – 0.264910514 × *SAMD1* + 0.532519618 × *C7* + 0.437584101 × *EDNRB* + 1.570842883 × *GPR34* + 1.656234352 × *SDS* + 1.773243073 × *STOM* + 1.685475222 × *VSTM4*. Kaplan-Meier survival analyses indicated that high-risk patients exhibited poorer survival outcomes in both the TCGA and GEO cohorts (*Figure 3F-3H*). Furthermore, the AUC values for the model ranged from 0.58 to 0.82 in the GSE58812 cohort, 0.62 to 0.84 in the meta cohort and 0.83 to 1 in the TCGA cohort, demonstrating its predictive capability (*Figure 3I-3K*).

Mutation and pathway analysis of the hub genes

We analyzed the SNV mutations of the risk signature's eight genes and observed that *ADGRF5*, *C7*, *EDNRB*, *GPR34*, *SAMD1*, *STOM*, and *VSTM4* had *SNV* (single-nucleotide variant) mutations in multiple samples. However, no SNV mutation was found in *SDS* (*Figure 4A*). We then examined the co-occurrence probability between these key genes and the 10 most mutated genes. *GPR34* showed a significant probability of co-occurrence with *TTN*, *MUC16*, and *APC* mutations (*Figure 4B*). Furthermore, we investigated the mutation frequency in ten major oncogenic pathways and detected mutations in several pathways, including PI3K, TP53, and RTK-RAS pathways (*Figure 4C*). Among the eight genes, only a few samples exhibited gain/loss of CNV (*Figure 4D*). To evaluate the tumor mutation burden (TMB), we calculated the TMB of TCGA patients and analyzed its distribution in the two risk groups. The waterfall plot visualized the top ten mutated genes (*Figure 4E*), and a significant difference in TMB was observed between the groups, with higher TMB in the low-risk group (*Figure 4F*). Additionally, we explored the co-occurrence probability of the five most mutated genes and found a significant probability of co-occurrence between *MUC16* and *TTN* (*Figure 4G*). Pathway analysis revealed that these eight genes were significantly correlated with 24 pathways, including base excision repair, prostate cancer, and gap junction (*Figures 4H*,*4I*). Moreover, immune-related pathways were found highly enriched in the high-risk group (*Figure 4J*).

Relationship between hub genes and immunity

In *Figure 5A*, the correlation between the immune score and the expression of the eight genes was presented. *GPR34*, *SDS*, *VSTM4*, *ADGRF5*, *C7*, *STOM*, and *EDNRB* showed significantly positive correlations with stromal score, immune score, and estimate score, while SAMD1 exhibited significantly negative correlations with these scores (*Figure 5B*). When grouping based on gene expression median values, we compared the immune score between different expression groups. The high-expression group of *C7*, *GPR34*, *SDS*, and *STOM* genes had significantly higher immune scores compared to the low-expression group (*Figure 5C*). Furthermore, *ADGRF5*, C7, *EDNRB*, and *VSTM4* were significantly positively correlated with mast cells resting, B cells naive, and Plasma cells (*Figure 5D*). *GPR34* expression showed a positive correlation with all ten immune cell types (*Figure 5E*).

The 8-gene signature displayed a substantial correlation with immune-related characteristics

To assess the differences in immune status between subtypes, we utilized ESTIMATION and ssGSEA. Immune cells and stromal cells were evaluated in the two risk groups, and their scores were combined to obtain the estimated score. The low-risk group had lower scores compared to the high-risk group, with significant differences between the groups (P<0.001) (*Figure 6A*). The correlation analysis between risk scores and immune scores, stromal scores, and estimated scores confirmed significant associations (*Figure 6B-6D*). The ssGSEA analysis revealed significant differences in immune cell scores between the two risk groups, with higher immune cell scores in the higher risk group, except for type 2 T helper cells, which scored higher in the lower risk group (*Figure 6E*). Moreover, the high-risk group exhibited higher levels of Tumor Regression Score (TRS), cytolytic activity (CYT), and interferon-γ (IFN-γ), indicating a more immunoreactive microenvironment in the TCGA dataset (*Figure 6F-6H*). Using the CIBERSORT method, we assessed the immune heterogeneity between the two subtypes and identified 22 different immune cell infiltrations. Patients with higher risk scores displayed

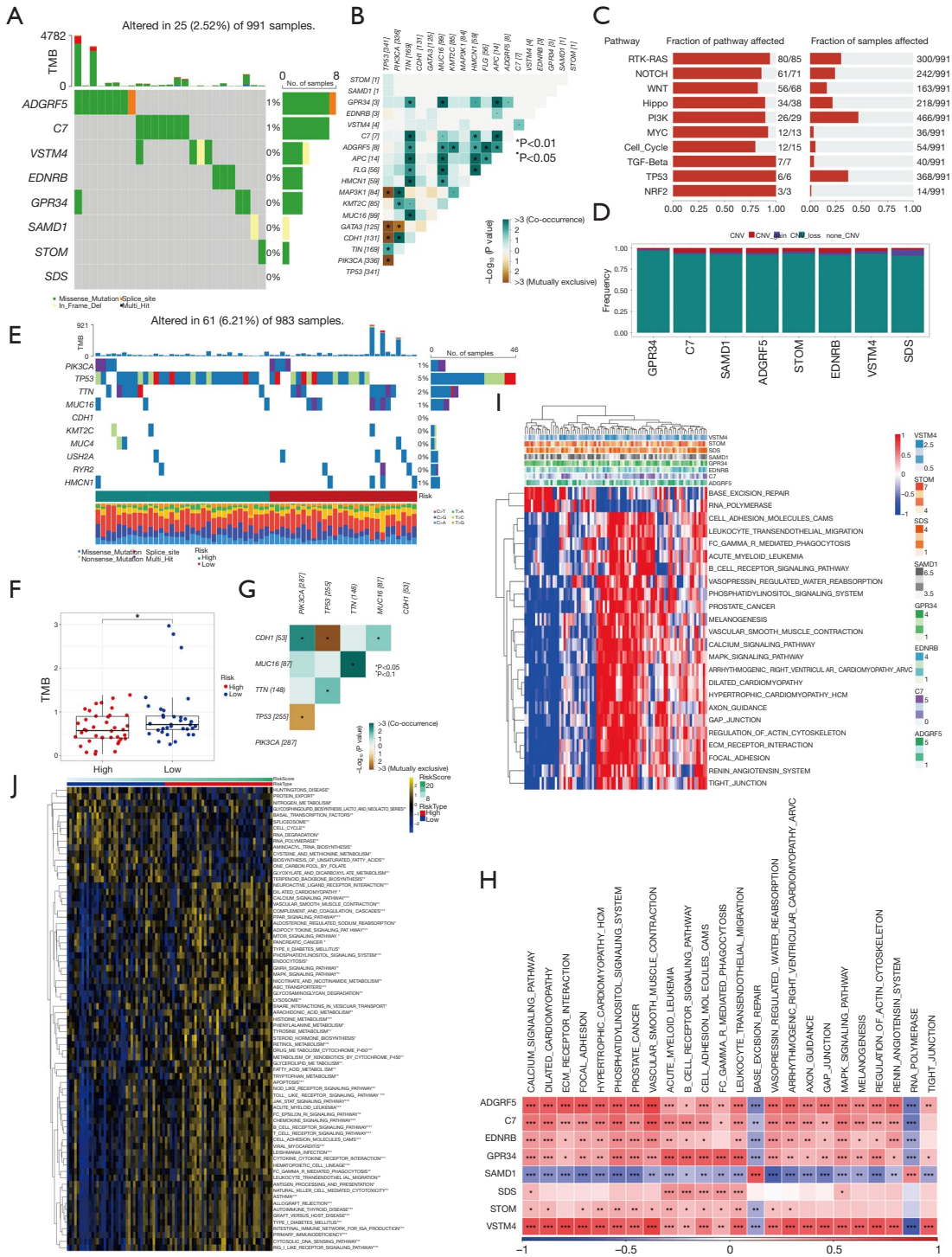

Figure 4 The characteristics of the mutations and identification of pathways that the risk genes involved in. (A) Waterfall diagram of SNV mutations of 8 key genes; (B) colinearity and mutual exclusion analysis of key genes and the 10 most mutated genes in tumors; (C) mutation frequency in 10 major oncogenic pathways; (D) CNV mutations (gain, loss, none) of 8 key genes; (E) waterfall plot of the top 10 mutated genes identified by calculating TMB; (F) TMB of two risk groups; (G) the co-occurrence probability of the 5 most mutated genes; (H) gene-pathway correlation heatmap; (I,J) enrichment score heatmap for key pathways. *, P<0.05; **, P<0.01; ***, P<0.001. SNV, single nucleotide variant; CNV, copy number variations; TMB, tumor mutational burden.

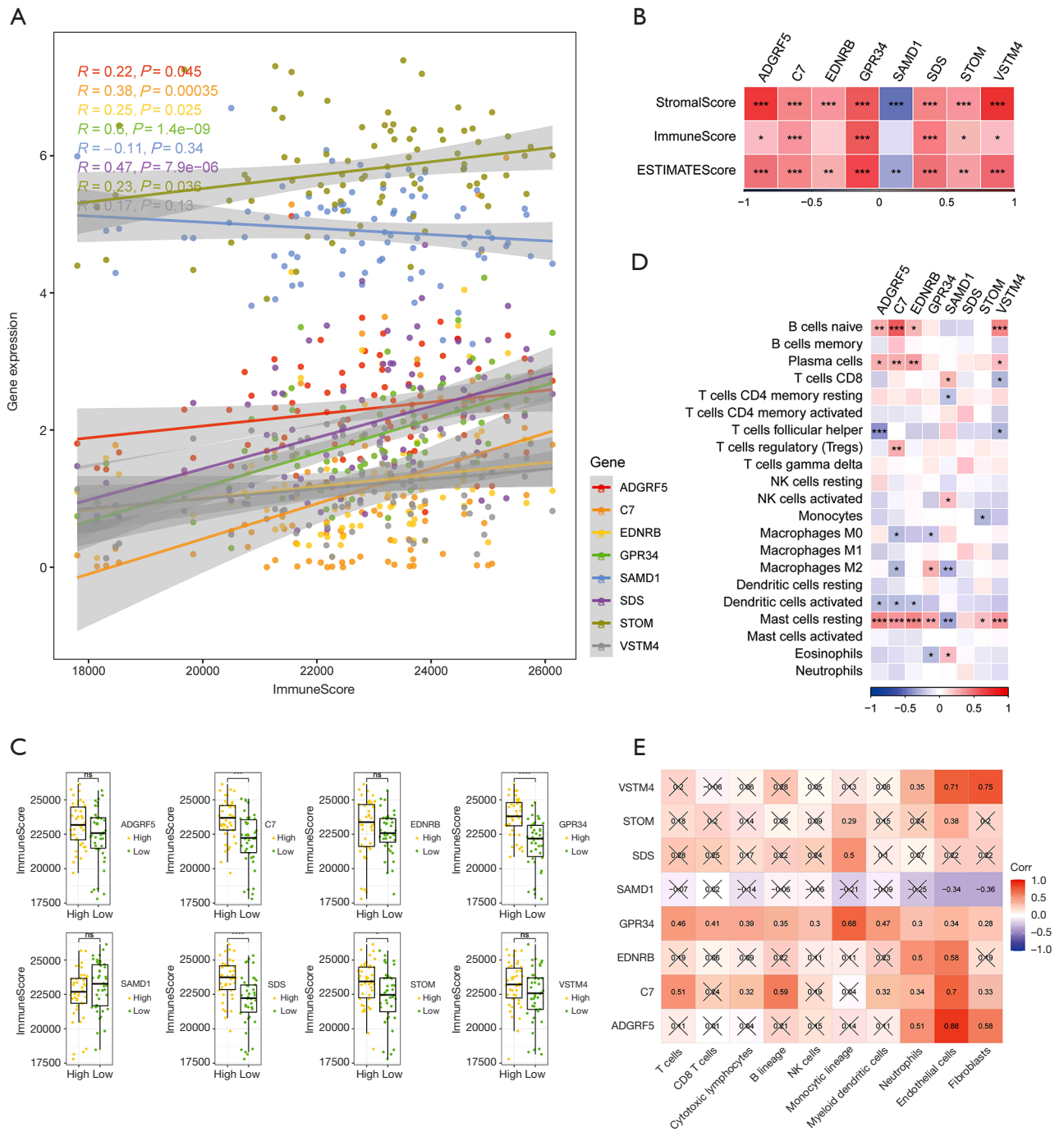

Figure 5 The relationship between the risk genes and immune landscape. (A) The correlation between immune score and the expression of risk genes; (B) the correlation of the risk genes and stromal score, immune score, and estimate score; (C) comparison of high and low expression of key genes and immune score; (D) correlation between key genes and immune cell score predicted by CIBERSORT analysis; (E) the correlation between the expression of risk genes and all of the 10 immune cells. *, P<0.05; **, P<0.01; ***, P<0.001; ns, not significant.

higher levels of B cells naive, T cells CD8, T cells regulatory (Tregs), monocytes, macrophages M1, macrophages M2, and mast cells resting, but lower proportions of T cells CD4 naive and Mast cells activated (*Figure 6I*). Additionally, we examined the expression levels of immune checkpoints in the two groups and found elevated levels in the high-risk subtype. Programmed cell death protein 1 (PD-1), PD-L1, and cytotoxic T lymphocyte-associated antigen-4 (CTLA4) showed significantly higher expression levels in the high-risk group (*Figure 6J-6K*). Furthermore, the results of Subclass Mapping (Submap) indicated that patients in the high-risk group were more likely to respond to ICIs (*Figure 6L*). Therefore, we can infer that the high-risk group belongs to the hot tumor subtype and may exhibit a favorable response to immunotherapy.

Identification of independent risk factors and potential therapeutic agents

To enhance the predictive performance of the risk signature, we conducted univariate and multivariate Cox regression analysis, integrating clinicopathological characteristics and risk scores. The multivariate analysis revealed that the risk signature emerged as the most significant independent prognostic factor for TNBC, with a hazard ratio (HR) of 3.683 [95% confidence interval (CI): 1.662–8.164, P=0.001]. Following closely was the stage, with an HR of 216.993 (95% CI: 2.585–18,218.507, P=0.02) (*Figure 7A*,*7B*). Consequently, we developed a nomogram by combining the stage and risk score, depicted in *Figure 7C*. The calibration plot demonstrated the effective predictive capability of the nomogram for actual survival outcomes (*Figure 7D*). Moreover, the DCA revealed that the nomogram exhibited superior discriminatory ability in identifying high-risk patients compared to the risk score and stage alone, as shown in *Figure 7E*. Time ROC analysis illustrated that the AUC of the risk score and nomogram surpassed that of other indicators in the TCGA cohort (*Figure 7F*). To identify potential agents for high-risk TNBC patients, we utilized sensitivity data from the Cancer Therapeutics Response Portal (CTRP) and profiling relative inhibition simultaneously in mixtures (PRISM) datasets, encompassing 481 compounds across 835 cancer cell lines (CCLs) and 1,448 compounds across 482 CCLs, respectively. Through this analysis, we identified 9 CTRP-derived agents (RITA, cytochalasin B, NVP-TAE684, GDC-0941, BRD-K63431240, birinapant, dasatinib, cucurbitacin I, and 1S, 3R-RSL-3) and 21 PRISM-derived agents (semaxanib, P276-00, AS-703026, trametinib, AMG-232, selumetinib, TAK-733, BVD-523, AZD8330, idasanutlin, PD-0325901, PD-184352, ponatinib, dasatinib, Ro-4987655, VS-4718, MEK162, PHA-848125, cobimetinib, tipifarnib, GDC-0152) (*Figure 7G*,*7H*). These agents exhibited estimated AUC values that were not only significantly negatively correlated with risk but also significantly lower in the high-risk group (*Figure 7I*,*7J*).

GPR34 mRNA and protein expression in TNBC

To explore *GPR34* as a potential biomarker for TNBC, we primally investigated *GPR34* mRNA and protein expression in MDA-MB-231 (TNBC cell line) compared with MCF-10A (normal breast epithelial cell line) via RT-PCR and western blot, respectively. Subsequently,

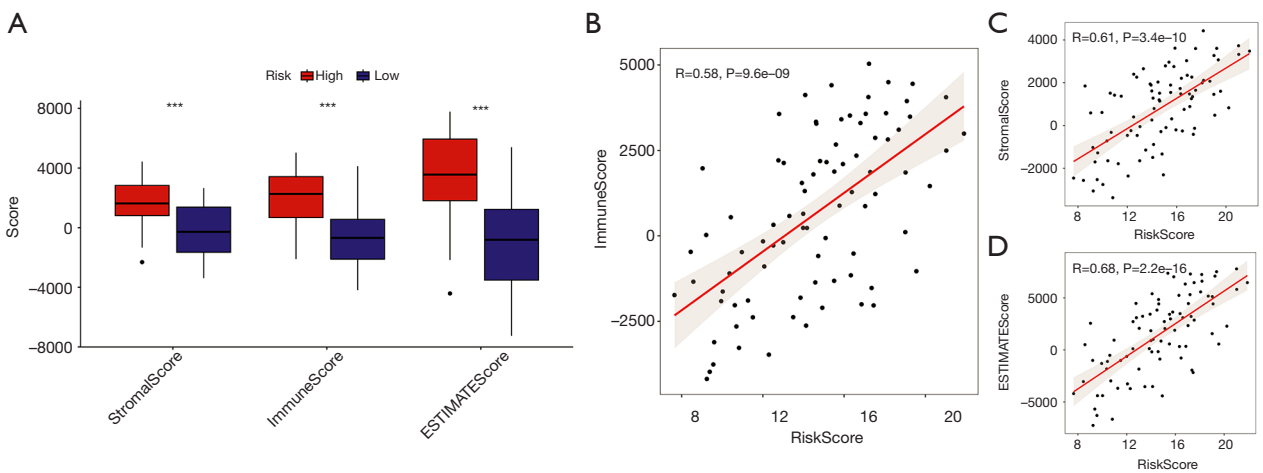

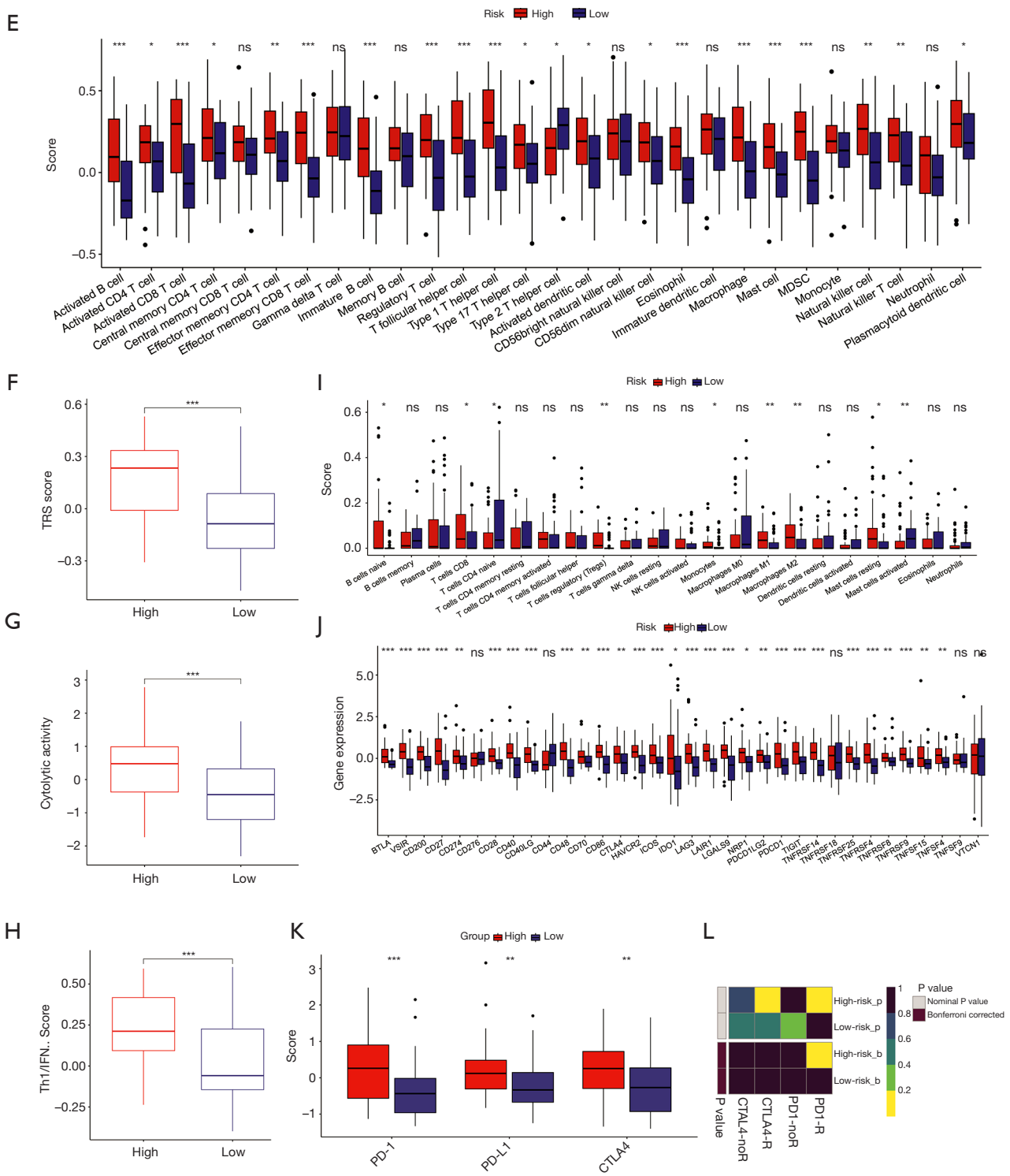

Figure 6 The correlation between our 8-gene signature and immune-related characteristics. (A-D) ESTIMATE analysis; (E-H) ssGSEA analysis; (I) CIBERSORT analysis; (J,K) exploration of immune checkpoints; (L) submap analysis. *, P<0.05; **, P<0.01; ***, P<0.001; ns, not significant. ssGSEA, single sample gene set enrichment analysis; TRS, Tumor Regression Score; MDSC, myeloid-derived suppressor cell.

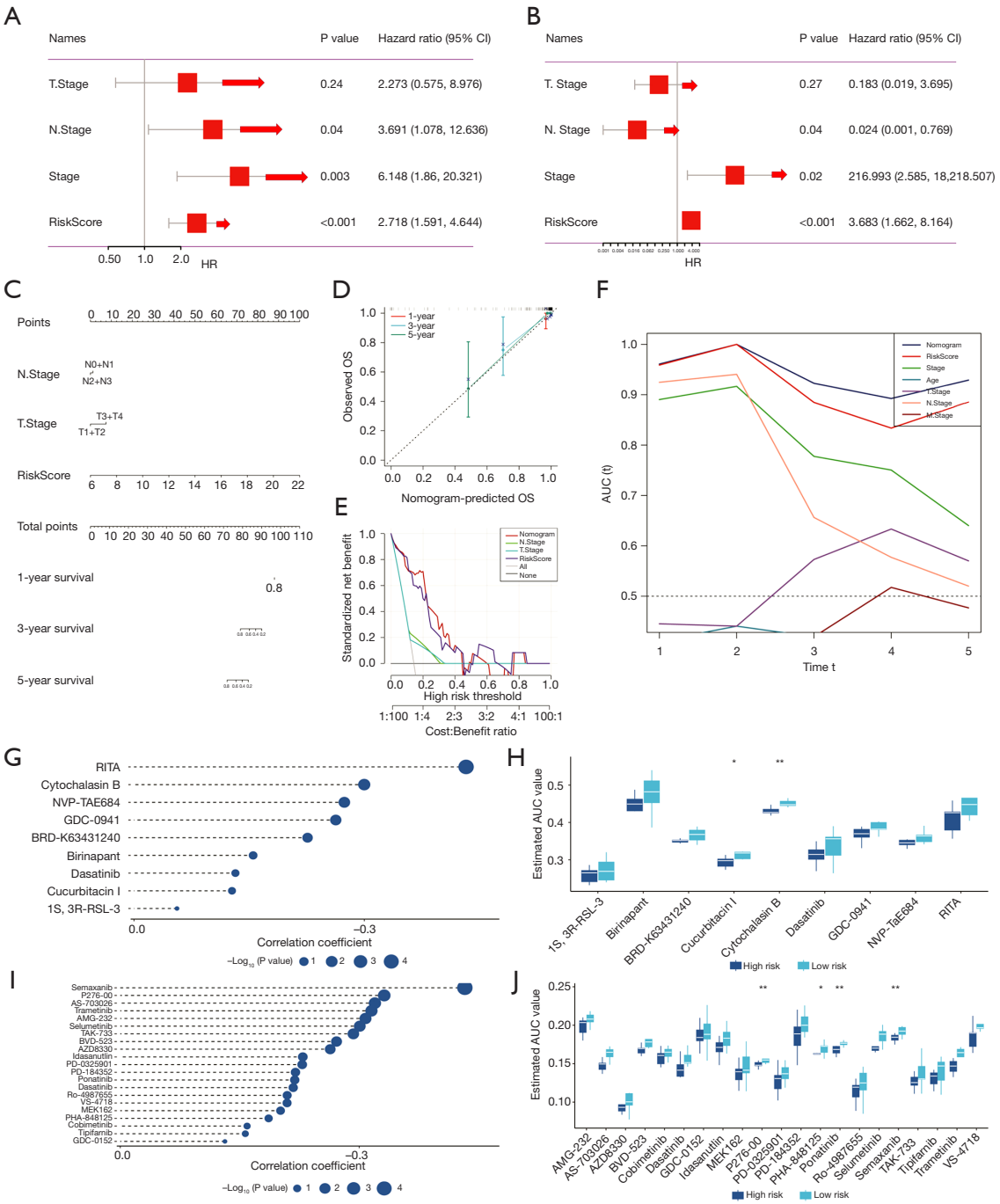

Figure 7 The development of a nomogram and Spearman's correlation analysis. (A,B) Univariate and multivariate Cox analysis displayed excellent predictive performance of our risk signature; (C) nomogram model integrating the risk score and stage was constructed; (D) calibration curves for 1, 3, and 5 years of nomogram; (E) decision curve for nomogram; (F) comparison of the predictive capacity of clinicopathological features and the nomogram using time-ROC analysis; (G-H) the results of Spearman's correlation analysis and differential drug response analysis of 9 CTRP-derived compounds; (I,J) the results of Spearman's correlation analysis and differential drug response analysis of 21 PRISM-derived compounds. Please be aware that reduced values along the y-axis of boxplots indicate higher sensitivity to the drug. *, P<0.05; **, P<0.01. CTRP, The Cancer Therapeutics Response Portal; PRISM, profiling relative inhibition simultaneously in mixtures; ROC, receiver operating characteristic; CI, confidence interval; OS, overall survival; AUC, area under the curve.

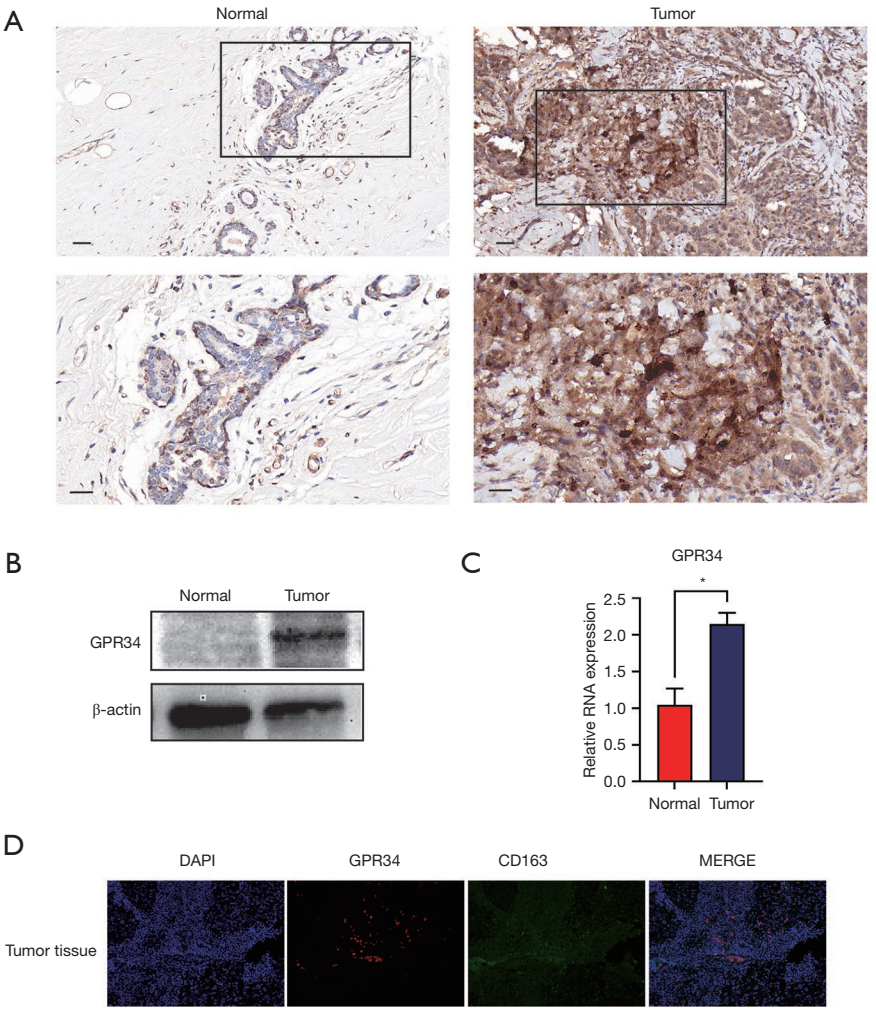

Figure 8 A series of experiments to verify the expression of GPR34. (A) IHC was used to examine GPR34 expression in tumor tissues and normal tissues. Scale bars: 20 μm (n>3). (B) Western blotting analysis of GPR34 expression in MDA-MB-231 cells compared with MCF-10A cells. (C) RT-PCR analysis of GPR34 expression in MDA-MB-231 cells compared with MCF-10A cells (n=3). (D) Immunofluorescence staining for GPR34 and CD163 in human breast cancer tissue. Tissues were stained with DAPI. Blue: DPAI. Red: GPR34. The green represents CD163. Scale bars, 100 μm (n>3). IHC, immunohistochemistry; GPR34, G protein-coupled receptor 34; RT-PCR, reverse-transcriptase polymerase chain reaction; DAPI, 4',6-diamidino-2'-phenylindole. *, P<0.05.

the differential expression of *GPR34* protein between TNBC tissue samples and normal breast tissue samples was performed by immunohistochemistry. Western blot and immunohistochemistry results also showed higher *GPR34* protein expression in MDA-MB-231 and TNBC tissues (*Figure 8A*,*8B*). The result of RT-PCR indicated increased *GPR34* mRNA expression in MDA-MB-231 (P=0.02, *Figure 8C*). Based on earlier research, *GPR34* has been found to be more highly expressed in macrophages. To further verify that *GPR34* expression is primarily localized to macrophages in tissues, we conducted immunofluorescence co-localization experiments using CD163 (markers of macrophages), and GPR34. As depicted in *Figure 8D*, the expression of *GPR34* was predominantly observed in macrophages.

Discussion

With emerging evidence uncovering the crucial role of the TME in tumor initiation, progression, therapeutic response, and resistance, the insight of cancer research gradually shifts from the tumor itself to the surrounding microenvironment (20,21). TME is a complex network

comprising a variety of immune cell types, endothelial cells, cancer-associated fibroblasts, and other tissue-resident cell types (22). TAMs represent a major component of the TME and have been proven to mediate tumor progression, poor prognosis, and therapy resistance in various malignancies (23,24). Recent research has provided evidence indicating the crucial involvement of TAMs in promoting the aggressive characteristics of TNBC, suggesting their potential as biomarkers for prognosis prediction (25,26). In TNBC, TAMs originate from circulating monocytes that are recruited by various signals released by the tumor and surrounding cells to the TME. Dynamic changes in TAMs subpopulations were observed during tumor development and correlated with immunotherapy's efficacy (24). TAMs exhibit diverse polarization states, typically categorized into M1 (pro-inflammatory) and M2 (anti-inflammatory) phenotypes. In TNBC, TAMs often polarize towards the M2 phenotype, which is associated with immunosuppression and promotion of tumor growth. TAMs contribute to TNBC progression mainly through secreting cytokines and growth factors that support tumor growth, angiogenesis, and tissue remodeling (27). Additionally, TAMs in TNBC can be reprogrammed by altering their environment or through targeted therapies. Reprogramming strategies aim to shift TAMs from a tumor-promoting M2 phenotype to a more anti-tumor M1 phenotype, thereby enhancing immune responses against the tumor. Understanding these aspects of TAM biology is crucial for developing effective therapeutic strategies targeting TAMs in TNBC (28).

TAMs heterogeneity in the TNBC TME is influenced by several molecular mechanisms. Cytokine and chemokine signaling: the TME secretes various cytokines and chemokines that influence macrophage polarization. For example, IL-6, IL-10, and TGF-β are associated with M2 polarization, which promotes immunosuppression and tumor progression. Transcriptional regulation: transcription factors such as STAT3, NF-κB, and PPARγ play key roles in shaping the macrophage phenotype. These factors can drive macrophages towards M2-like states in the presence of tumor-derived signals (29). Metabolic pathways: metabolic changes within the TME, such as hypoxia and altered nutrient availability, can affect macrophage polarization and function. For instance, hypoxic conditions can lead to increased expression of HIF-1α, promoting M2 polarization. Epigenetic modifications: epigenetic changes, including DNA methylation and histone modifications, can also influence macrophage identity and function in TNBC. Macrophages play different roles in TNBC progression (30). TAMs are involved in the whole process of breast cancer development. In the early stages of TNBC, macrophages can contribute to tumor initiation through the secretion of pro-inflammatory cytokines and growth factors that support early tumor cell survival and proliferation. In the intermediate stage, as the tumor progresses, macrophages play a role in promoting tumor growth and angiogenesis. They secrete factors that enhance blood vessel formation and support tumor expansion. In the advanced Stage, macrophages often adopt an M2-like phenotype, contributing to immune evasion, metastasis, and resistance to therapy. They can create an immunosuppressive microenvironment that hinders effective anti-tumor responses (31).

Moreover, dynamic changes in TAMs subpopulations were observed during tumor development and were correlated with the efficacy of immunotherapy (24). In this study, we conducted a comprehensive investigation of the characteristics and classification of TAMs in TNBC using scRNA-seq data. We identified a total of four distinct TAM clusters and further examined the correlation between these clusters and the prognosis of TNBC. In our analysis, the cluster TAM-0 showed a unique prognostic value compared with other TAM clusters, which illustrated that specific TAM clusters may have potential prognostic prediction and help find new prognostic subtyping patterns for TNBC.

Based on DEGs identified within the TAMs clusters, which were significantly associated with TNBC prognosis, we developed a risk signature specifically based on TAMs. The signature is composed of six risk genes (*C7*, *EDNRB*, *GPR34*, *SDS*, *STOM*, and *VSTM4*), and two protective genes (ADGRF5 and SAMD1). The report has revealed that high expression of *C7* in breast cancer indicates poor prognosis of breast cancer and inhibits sensitivity to taxane-anthracycline chemotherapy (32). *STOM* is also dedicated to participating in the metastasis of breast cancer (33). G-protein coupled receptor 34 (*GPR34*), which is one member of the G-protein coupled receptor superfamily, is reported to participate in certain cellular physiological functions such as cell growth, differentiation, and motility (34). *GPR34* has also been demonstrated to promote the malignant phenotype of certain cancers, including cervical cancer, gastric adenocarcinoma, and colorectal cancer (34,35). Elevated expression of *GPR34* has been detected in cell lines of cervical cancer and colorectal cancer (36-38). Consistent with these results, *GPR34* also showed a higher presentation in TNBC tissues and MDA-MB-231 cells in our study. Additionally, our findings demonstrated a stronger immune

association between *GPR34* and TNBC, in contrast to the other seven hub genes. Earlier investigations have also highlighted the significance of *GPR34* in immune responses, emphasizing its role in stimulating paracrine signaling in malignant B cells (35,39). Therefore, we hypothesized that *GPR34* might be involved in the immune-related malignant characteristics of TNBC and could serve as a promising immunotherapy target. This hypothesis requires further investigation. Additionally, we examined the association between the signature and the prognosis of TNBC. The results revealed that the high-risk group had a poorer prognosis, demonstrating the division of the risk signature into high- and low-risk groups. Our findings suggest that the risk signature represents a dependable tool for precise prognosis prediction in TNBC patients. In addition, mutation and pathway analysis of the hub genes were then performed. We found almost all genes had SNV mutations and three oncogenic pathways (PI3K, TP53, and RTK-RAS) were selected. Since its discovery in 1985, the PI3K pathway has remained a prominent and extensively studied target for therapeutic intervention (40). PI3K is a kinase that was first uncovered to involve cellular transformation for its association with polyoma middle T antigens and was later found to play an important role in human cancers for its activity in mitogenesis and oncogenesis (41). PI3K is known to regulate essential cellular functions, including protein synthesis, glucose metabolism, cell apoptosis, and survival. This is achieved through the generation of phosphatidylinositol 3,4,5-trisphosphate (PIP3), which acts as a potent second messenger, recruiting specific kinases like AKT and PDPK1 to the plasma membrane (41). The advent of cancer genome sequencing has shed light on PI3K mutations in various human cancers, such as breast, colorectal, gastric, and lung tumors, in the 2000s (42). Several drugs targeting the PI3K pathway have gained regular or accelerated approval from the FDA for the treatment of PIK3CA-mutant, estrogen receptor-positive advanced-stage breast cancer (41). It is illustrated that TNBC harbors mutations in the PI3K that may tend to occur progression and therapy resistance (43,44). The latest research illustrated that activating the PI3K/AKT pathway may induce chemotherapeutic resistance in TNBC. Moreover, TMB analysis suggested higher TMB in the low-risk group. These findings indicated that our risk signature may play an important role in the development and therapeutic response of TNBC and might provide a basis for exploring new therapeutic targets for TNBC. The rapid advancement of immunotherapy has provided a new perspective on cancer treatment, emphasizing the crucial importance of understanding the immune landscape within the TME (45,46). The TME exerts a profound influence on cancer biology and can greatly affect the efficacy of therapeutic interventions (47). TAM has been described to be intimately involved in immunosuppression and influences immunotherapy in many cancers (48,49). Targeting markers on tumor-associated macrophages could enhance cancer immunotherapy (50). TAMs have also been shown to modulate PD-1/PD-L1 presentation in the TME of TNBC directly and indirectly (51). Our study then mainly analyzed immune characteristics of the risk signature in TNBC and the results showed that immune-related pathways were found highly enriched in the high-risk group. Calculating immune scores of the 8 hub genes, the high expression group had significantly higher immune scores. The ssGSEA analysis and the CIBERSORT method revealed significant differences in immune cell scores and immune cell correlation among the two risk groups, respectively. In addition, the high-risk group exhibited higher levels of TRS, CYT, and IFN-γ which represent a more immunoreactive microenvironment. Subsequently, the increased expression levels of immune checkpoints including PD-1, PD-L1, and CTLA4 in the high-risk subtype were evaluated. These studies suggest an important immunological value of our risk signature. We, therefore, explored potential immunotherapy drugs based on the signature. Consequently, 9 CTRP-derived agents and 21 PRISM-derived agents were found. CTRP-derived GDC-0941 is PI3K inhibitor and PI3K is an important component and has been found aberrant in signaling pathways related to cellular biological functions including growth, survival, metabolism, and genomic stability in several malignancies, breast cancer included (52). Despite previous findings indicating the restricted therapeutic efficacy of GDC-0941 in TNBC, recent *in vitro* investigations propose that co-administration of the third-generation retinoid adapalene (ADA) with GDC-0941 could enhance TNBC's responsiveness to GDC, leading to suppressed tumor growth and diminished treatment resistance (52,53). Our signature may provide novel strategies for the improvement of existing immunotherapy and further immunotherapy exploration in TNBC.

Our study does have limitations. First, this risk signature was constructed mainly based on retrospective data and prospective studies remain to be performed. Second, our experiments focus on histological and cellular level research, while animal-level experiments need to be conducted in

the future. Last but not least, the underlying mechanism by which this risk signature participates in the prognosis and immunity of TNBC patients has not been revealed and we shall carry out further exploration of it based on both bioinformatics and experiments.

In conclusion, this exploration is an important attempt at TAM clusters-related risk signature in TNBC, providing unique value for finding independent prognostic factors, updating immunotherapy methods, and finding effective therapeutic targets.

Conclusions

This study characterized the TAM populations in TNBC and generated 4 TAM clusters with distinct diversity. All the clusters were significantly associated with TNBC prognosis and used to construct a TAM-based prognostic risk signature with 8 genes. The TAM-based gene signature was observed to be connected with the immune landscape and could be used to predict responsiveness to PD-L1 blockade immunotherapy. Finally, a novel nomogram integrating the risk signature and clinicopathological features was developed, which provided a favorable predictive performance in the clinical outcome of patients with TNBC.

Acknowledgments

The authors thank the patients and their families for their support.
Funding: This study was supported by the Nantong Municipal Science and Technology Bureau.

Footnote

Reporting Checklist: The authors have completed the MDAR and TRIPOD reporting checklists. Available at https://tcr.amegroups.com/article/view/10.21037/tcr-24-1037/rc

Data Sharing Statement: Available at https://tcr.amegroups.com/article/view/10.21037/tcr-24-1037/dss

Peer Review File: Available at https://tcr.amegroups.com/article/view/10.21037/tcr-24-1037/prf

Conflicts of Interest: All authors have completed the ICMJE uniform disclosure form (available at https://tcr.amegroups.com/article/view/10.21037/tcr-24-1037/coif). The authors have no conflicts of interest to declare.

Ethical Statement: The authors are accountable for all aspects of the work in ensuring that questions related to the accuracy or integrity of any part of the work are appropriately investigated and resolved. The study was conducted in accordance with the Declaration of Helsinki (as revised in 2013).

References

1. Nolan E, Lindeman GJ, Visvader JE. Deciphering breast cancer: from biology to the clinic. Cell 2023;186:1708-28.
2. Leon-Ferre RA, Goetz MP. Advances in systemic therapies for triple negative breast cancer. BMJ 2023;381:e071674.
3. Liedtke C, Mazouni C, Hess KR, et al. Response to Neoadjuvant Therapy and Long-Term Survival in Patients With Triple-Negative Breast Cancer. J Clin Oncol 2023;41:1809-15.
4. Liu Y, Zhu XZ, Xiao Y, et al. Subtyping-based platform guides precision medicine for heavily pretreated metastatic triple-negative breast cancer: The FUTURE phase II umbrella clinical trial. Cell Res 2023;33:389-402.
5. Oliveira G, Wu CJ. Dynamics and specificities of T cells in cancer immunotherapy. Nat Rev Cancer 2023;23:295-316.
6. Agnello L, d'Argenio A, Nilo R, et al. Aptamer-Based Strategies to Boost Immunotherapy in TNBC. Cancers (Basel) 2023;15:2010.
7. Tarantino P, Antonarelli G, Ascione L, et al. Investigational immunomodulatory drugs for enhancement of triple negative breast cancer (TNBC) immunotherapy: early phase development. Expert Opin Investig Drugs 2022;31:499-513.
8. He S, Song W, Cui S, et al. Modulation of miR-146b by N6-methyladenosine modification remodels tumor-associated macrophages and enhances anti-PD-1 therapy in colorectal cancer. Cell Oncol (Dordr) 2023;46:1731-46.
9. Wu H, Feng J, Zhong W, et al. Model for predicting immunotherapy based on M2 macrophage infiltration in TNBC. Front Immunol 2023;14:1151800.

10. Sami E, Paul BT, Koziol JA, et al. The Immunosuppressive Microenvironment in BRCA1-IRIS-Overexpressing TNBC Tumors Is Induced by Bidirectional Interaction with Tumor-Associated Macrophages. Cancer Res 2020;80:1102-17.
11. Timperi E, Gueguen P, Molgora M, et al. Lipid-Associated Macrophages Are Induced by Cancer-Associated Fibroblasts and Mediate Immune Suppression in Breast Cancer. Cancer Res 2022;82:3291-306.
12. Mariathasan S, Turley SJ, Nickles D, et al. TGFβ attenuates tumour response to PD-L1 blockade by contributing to exclusion of T cells. Nature 2018;554:544-8.
13. Butler A, Hoffman P, Smibert P, et al. Integrating single-cell transcriptomic data across different conditions, technologies, and species. Nat Biotechnol 2018;36:411-20.
14. Chi H, Peng G, Yang J, et al. Machine learning to construct sphingolipid metabolism genes signature to characterize the immune landscape and prognosis of patients with uveal melanoma. Front Endocrinol (Lausanne) 2022;13:1056310.
15. Ritchie ME, Phipson B, Wu D, et al. limma powers differential expression analyses for RNA-sequencing and microarray studies. Nucleic Acids Res 2015;43:e47.
16. Chen B, Khodadoust MS, Liu CL, et al. Profiling Tumor Infiltrating Immune Cells with CIBERSORT. Methods Mol Biol 2018;1711:243-59.
17. Danilova L, Ho WJ, Zhu Q, et al. Programmed Cell Death Ligand-1 (PD-L1) and CD8 Expression Profiling Identify an Immunologic Subtype of Pancreatic Ductal Adenocarcinomas with Favorable Survival. Cancer Immunol Res 2019;7:886-95.
18. Charoentong P, Finotello F, Angelova M, et al. Pan-cancer Immunogenomic Analyses Reveal Genotype-Immunophenotype Relationships and Predictors of Response to Checkpoint Blockade. Cell Rep 2017;18:248-62.
19. Zhang S, Tong YX, Zhang XH, et al. A novel and validated nomogram to predict overall survival for gastric neuroendocrine neoplasms. J Cancer 2019;10:5944-54.
20. Liu Y, Tiruthani K, Wang M, et al. Tumor-targeted gene therapy with lipid nanoparticles inhibits tumor-associated adipocytes and remodels the immunosuppressive tumor microenvironment in triple-negative breast cancer. Nanoscale Horiz 2021;6:319-29.
21. Sherman MH, Beatty GL. Tumor Microenvironment in Pancreatic Cancer Pathogenesis and Therapeutic Resistance. Annu Rev Pathol 2023;18:123-48.
22. de Visser KE, Joyce JA. The evolving tumor microenvironment: From cancer initiation to metastatic outgrowth. Cancer Cell 2023;41:374-403.
23. Pan Y, Yu Y, Wang X, et al. Tumor-Associated Macrophages in Tumor Immunity. Front Immunol 2020;11:583084.
24. Xiang X, Wang J, Lu D, et al. Targeting tumor-associated macrophages to synergize tumor immunotherapy. Signal Transduct Target Ther 2021;6:75.
25. Chen X, Yang M, Yin J, et al. Tumor-associated macrophages promote epithelial-mesenchymal transition and the cancer stem cell properties in triple-negative breast cancer through CCL2/AKT/β-catenin signaling. Cell Commun Signal 2022;20:92.
26. Qiu X, Zhao T, Luo R, et al. Tumor-Associated Macrophages: Key Players in Triple-Negative Breast Cancer. Front Oncol 2022;12:772615.
27. Nalio Ramos R, Missolo-Koussou Y, Gerber-Ferder Y, et al. Tissue-resident FOLR2(+) macrophages associate with CD8(+) T cell infiltration in human breast cancer. Cell 2022;185:1189-1207.e25.
28. Xia J, Zhang L, Peng X, et al. IL1R2 Blockade Alleviates Immunosuppression and Potentiates Anti-PD-1 Efficacy in Triple-Negative Breast Cancer. Cancer Res 2024;84:2282-96.
29. Wang S, Li J, Hong S, et al. Chemotherapy-elicited extracellular vesicle CXCL1 from dying cells promotes triple-negative breast cancer metastasis by activating TAM/PD-L1 signaling. J Exp Clin Cancer Res 2024;43:121.
30. Emami F, Pathak S, Nguyen TT, et al. Photoimmunotherapy with cetuximab-conjugated gold nanorods reduces drug resistance in triple negative breast cancer spheroids with enhanced infiltration of tumor-associated macrophages. J Control Release 2021;329:645-64.
31. Hirano R, Okamoto K, Shinke M, et al. Tissue-resident macrophages are major tumor-associated macrophage resources, contributing to early TNBC development, recurrence, and metastases. Commun Biol 2023;6:144.
32. Zhang H, Zhao Y, Liu X, et al. High Expression of Complement Component C7 Indicates Poor Prognosis of Breast Cancer and Is Insensitive to Taxane-Anthracycline Chemotherapy. Front Oncol 2021;11:724250.
33. Duan J, Bao C, Xie Y, et al. Targeted core-shell nanoparticles for precise CTCF gene insert in treatment of metastatic breast cancer. Bioact Mater 2021;11:1-14.
34. Cheng Y, Heng X, Feng F. G-protein Coupled Receptor 34 Promotes Gliomagenesis by Inducing

Proliferation and Malignant Phenotype via TGF-Beta/Smad Signaling Pathway. Technol Cancer Res Treat 2022;21:15330338221105733.
35. Schöneberg T, Meister J, Knierim AB, et al. The G protein-coupled receptor GPR34 - The past 20 years of a grownup. Pharmacol Ther 2018;189:71-88.
36. Tan Y, Wang H, Zhang C. MicroRNA-381 targets G protein-Coupled receptor 34 (GPR34) to regulate the growth, migration and invasion of human cervical cancer cells. Environ Toxicol Pharmacol 2021;81:103514.
37. Wang M, Tian Y, Miao L, et al. MicroRNA-300 Inhibits the Proliferation and Metastasis of Cervical Cancer Cells via Posttranscriptional Suppression of G Protein-Coupled Receptor 34 (GPR34). J Oncol 2021;2021:2669822.
38. Iida Y, H Tsuno N, Kishikawa J, et al. Lysophosphatidylserine stimulates chemotactic migration of colorectal cancer cells through GPR34 and PI3K/Akt pathway. Anticancer Res 2014;34:5465-72.
39. Korona B, Korona D, Zhao W, et al. GPR34 activation potentially bridges lymphoepithelial lesions to genesis of salivary gland MALT lymphoma. Blood 2022;139:2186-97.
40. Whitman M, Kaplan DR, Schaffhausen B, et al. Association of phosphatidylinositol kinase activity with polyoma middle-T competent for transformation. Nature 1985;315:239-42.
41. Vasan N, Cantley LC. At a crossroads: how to translate the roles of PI3K in oncogenic and metabolic signalling into improvements in cancer therapy. Nat Rev Clin Oncol 2022;19:471-85.
42. Samuels Y, Wang Z, Bardelli A, et al. High frequency of mutations of the PIK3CA gene in human cancers. Science 2004;304:554.
43. Eustace AJ, Lee MJ, Colley G, et al. Aberrant calcium signalling downstream of mutations in TP53 and the PI3K/AKT pathway genes promotes disease progression and therapy resistance in triple negative breast cancer. Cancer Drug Resist 2022;5:560-576.
44. Wang W, Han D, Cai Q, et al. MAPK4 promotes triple negative breast cancer growth and reduces tumor sensitivity to PI3K blockade. Nat Commun 2022;13:245.
45. Zheng Y, Chen Z, Han Y, et al. Immune suppressive landscape in the human esophageal squamous cell carcinoma microenvironment. Nat Commun 2020;11:6268.
46. Ren Q, Zhang P, Zhang X, et al. A fibroblast-associated signature predicts prognosis and immunotherapy in esophageal squamous cell cancer. Front Immunol 2023;14:1199040.
47. Dinh HQ, Pan F, Wang G, et al. Integrated single-cell transcriptome analysis reveals heterogeneity of esophageal squamous cell carcinoma microenvironment. Nat Commun 2021;12:7335.
48. Li W, Wu F, Zhao S, et al. Correlation between PD-1/PD-L1 expression and polarization in tumor-associated macrophages: A key player in tumor immunotherapy. Cytokine Growth Factor Rev 2022;67:49-57.
49. Yan S, Wan G. Tumor-associated macrophages in immunotherapy. FEBS J 2021;288:6174-86.
50. Binnewies M, Pollack JL, Rudolph J, et al. Targeting TREM2 on tumor-associated macrophages enhances immunotherapy. Cell Rep 2021;37:109844.
51. Santoni M, Romagnoli E, Saladino T, et al. Triple negative breast cancer: Key role of Tumor-Associated Macrophages in regulating the activity of anti-PD-1/PD-L1 agents. Biochim Biophys Acta Rev Cancer 2018;1869:78-84.
52. Mehraj U, Wani NA, Hamid A, et al. Adapalene inhibits the growth of triple-negative breast cancer cells by S-phase arrest and potentiates the antitumor efficacy of GDC-0941. Front Pharmacol 2022;13:958443.
53. Mehraj U, Alshehri B, Khan AA, et al. Expression Pattern and Prognostic Significance of Chemokines in Breast cancer: An Integrated Bioinformatics Analysis. Clin Breast Cancer 2022;22:567-78.

Cite this article as: Miao S, Bian C, Fang J, Wang S, You H, Zhou Y, Ni Q. Integrated analysis reveals prognostic correlation and immune characteristics of a tumor-associated macrophage-based risk signature in triple-negative breast cancer. Transl Cancer Res 2024;13(10):5214-5232. doi: 10.21037/tcr-24-1037